GEOPHYSICS, VOL. 83, NO. 1 (JANUARY-FEBRUARY 2018); P. D9–D16, 13 FIGS., 1 TABLE.
10.1190/GEO2017-0300.1

Detection of formation S-wave in a slow formation using a monopole acoustic logging-while-drilling tool

Xinding Fang[1] and Arthur Cheng[2]

ABSTRACT

Acoustic logging-while-drilling (LWD) is a technology that is used to measure formation elastic properties during drilling. When the formation shear slowness is smaller than the borehole fluid slowness (i.e., fast formation), monopole logging can be used to obtain formation compressional and shear slownesses by measuring the corresponding refracted waves. In a slow formation in which the shear slowness is larger than the borehole fluid slowness, other logging methods, such as quadrupole LWD, are used instead for shear slowness measurement due to the lack of a fully refracted S-wave. Through modeling analysis, we find that the transmitted S-wave generated by a monopole LWD tool in a slow formation can be detected and used to measure the formation shear slowness. This phenomenon can be explained by Huygens' principle, which states that every point on a wavefront can be considered as a secondary source that induces particle motion. It is hard to discern the transmitted S-wave in monopole wireline data because it strongly interferes with the Stoneley mode in wireline logging. However, the transmitted S-wave decouples from the Stoneley in the LWD environment because the drill collar slows down the low-frequency part of the Stoneley mode. The nondispersive nature of the transmitted S-wave makes it suitable for shear slowness extraction using time semblance analysis, but sophisticated signal preprocessing might be needed because this wave is generally weak compared with the Stoneley wave. Moreover, our study helps us better understand how the Stoneley mode behaves and interferes with other modes in a slow formation under LWD conditions.

INTRODUCTION

Acoustic logging-while-drilling (LWD) technology is used to measure the formation elastic properties during drilling. Depending on the type of source used to excite acoustic energy in a borehole, conventional acoustic LWD can be divided into three major categories: monopole, dipole, and quadrupole (Tang and Cheng, 2004; Zhu et al., 2008). Using a monopole LWD tool, the compressional and shear slownesses can be measured from the corresponding P- and S-waves refracted along the wellbore when the formation shear slowness is below the borehole fluid slowness (called the fast formation). However, the shear slowness cannot be directly measured from monopole logging in a slow formation in which the formation shear slowness is larger than the borehole fluid slowness because there is no refracted S-wave (Tang et al., 2004; Wang et al., 2015). Because of the need for measuring shear slowness in slow formations, dipole and quadrupole tools were developed. Historically, due to the success of dipole tools in wireline logging, the dipole LWD tool was first developed and tested for shear measurements (Varsamis et al., 1999). However, the application of a dipole source under the LWD conditions was found to have two serious drawbacks caused by the drill collar: (1) strong tool mode contamination and (2) large slowness difference between formation shear and dipole flexural waves (Tang et al., 2002). To overcome the problems associated with the dipole LWD tool, the quadrupole tool was developed as a substitute for the dipole tool in LWD logging (Tang et al., 2002; Wang and Tang, 2003b). The advantage of using the quadrupole wave is that the collar mode exists only above the cutoff frequency (>10 kHz), so it does not affect the low-frequency formation quadrupole wave, which is used for determining shear slowness (Tang et al., 2002). Another type of LWD tool called the unipole was put into use in recent years (Wang et al., 2011; Syresin et al., 2016). A unipole tool has the transmitter and receivers on a single side of the tool; thus, it has the capability to measure the azimuthal variations in formation properties as the tool rotates while drilling.

Manuscript received by the Editor 11 May 2017; revised manuscript received 1 August 2017; published ahead of production 23 September 2017; published online 14 November 2017.
[1]Southern University of Science and Technology, Department of Earth and Space Sciences, Shenzhen, China. E-mail: fangxd@sustc.edu.cn.
[2]National University of Singapore, Department of Civil and Environmental Engineering, Singapore, Singapore. E-mail: arthurcheng@alum.mit.edu.

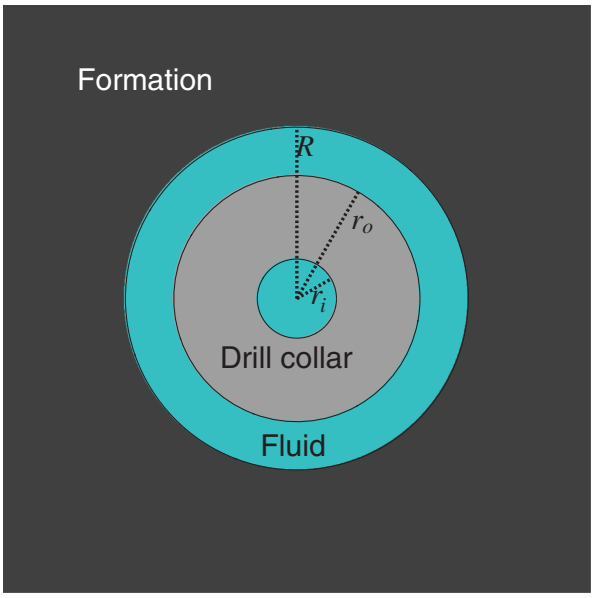

Figure 1. Configuration of the LWD model. The LWD tool is represented as a drill collar made of steel. The borehole radius is R. The inner and outer radii of the tool (i.e., drill collar) are r_i and r_o, respectively.

Table 1. Parameters for the LWD model.

	Compressional slowness (μs/ft)	Shear slowness (μs/ft)	Density (kg/m^3)	Radius (cm)
Inner fluid	207	0	1000	2.7
Drill collar	52	95	7850	8.4
Outer fluid	207	0	1000	11.7
Formation	139	272	2200	N/A

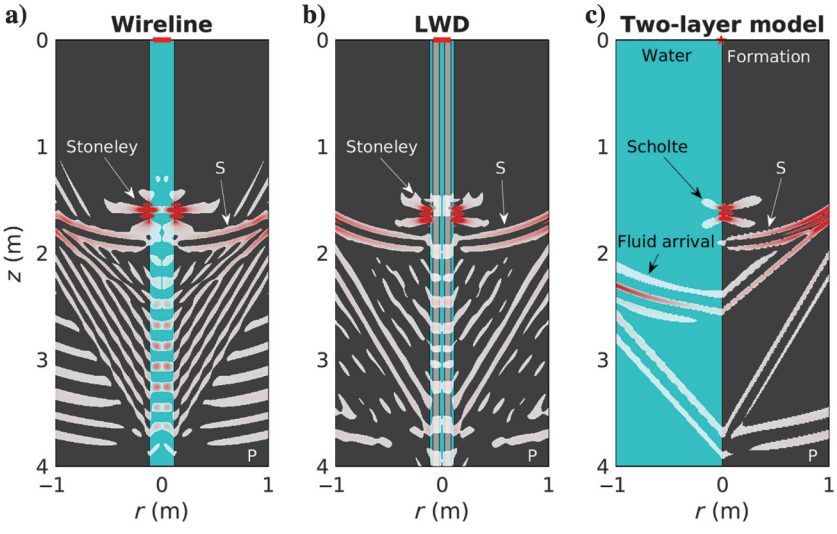

Figure 2. (a and b) Snapshots of the radial velocity component at 1.7 ms in the wireline and LWD models. P and S denote the P- and transmitted S-waves, respectively. The monopole source is located at $z = 0$ m. (c) A two-layer model for comparison. A point explosive source (star) is placed in the fluid 1 cm away from the fluid-solid boundary.

The quadrupole wave is dispersive, and its slowness is equal to the formation shear slowness only near the cutoff frequencies (Chen, 1989; Tang and Cheng, 2004; Jørgensen and Burns, 2013). Thus, evaluation of formation shear slowness using quadrupole data requires a model-based inversion approach that takes into account the dispersion of quadrupole modes (Zhang et al., 2010; Su et al., 2013). However, the inversion is not necessary to give the true answer in some situations because the dispersion behavior of quadrupole waves may not be reliable due to hardware limitations or operational problems. Therefore, a data-based approach for slow formation shear measurements is still desirable.

Although it is well-known that slow formations do not generate the refracted S-wave, the outgoing source energy can always produce a transmitted S-wave that propagates into the formation at the wellbore. We discover that the transmitted S-wave generated by a monopole LWD tool in a slow formation is detectable inside the borehole, although it is generally weak compared with other signals. This contradicts our understanding about borehole S-wave propagation in a slow formation. We will investigate this phenomenon in detail.

MODELING ANALYSIS

Our analysis focuses on investigating the characteristics of the borehole transmitted S-wave generated by a monopole acoustic source in a slow formation. Figure 1 shows a schematic of the LWD model. The model is axisymmetric. The material properties and model geometric parameters are listed in Table 1. The formation around the borehole is homogeneous and has elastic isotropy. The borehole radius R is 11.7 cm. The inner r_i and outer r_o radii of the LWD tool, which is represented as a steel collar, are 2.7 and 8.4 cm, respectively. For comparison, we also study the corresponding wireline case, in which the model is an open, fluid-filled borehole. Because the model properties are azimuthally invariant, a 2D staggered-grid finite-difference method (Wang and Tang, 2003a) can be used to simulate the borehole wave propagation in the r-z cylindrical coordinates. In all of the following simulations, the grid size is 3 mm and the time sampling is 0.25 μs. Validation of the finite-difference program is presented by Fang et al. (2014). The first receiver is 2 m away from the source, and an additional 33 receivers with 3 cm spacing are positioned at distances between 2 and 3 m. To avoid aliasing in the analysis, the receiver array used in the simulation is much denser than that in a real sonic tool. A perfectly matched layer absorbing boundary condition is added to all boundaries of the model. The monopole source is modeled as a ring source mounted on the tool surface. The source wavelet is a Ricker wavelet. A receiver array extending along the borehole axis direction is also placed on the surface of the tool.

Figure 2 shows snapshots of the wavefield (radial velocity component) at 1.7 ms in the wireline (Figure 2a) and LWD (Figure 2b) models together with a two-layer model (Figure 2c) for comparison. The source center frequency is 8 kHz. The only difference between the models in Figure 2a and 2b is the presence of the tool in the LWD model. In Figure 2c, the properties of

the fluid and solid layers are the same as those of the borehole fluid and formation in the other two models. In the two-layer model, the transmitted S-wave is very strong inside the formation. It is also detectable in the fluid near the interface because a portion of the shear energy leaks into the fluid. The strong interface wave arriving after the transmitted S-wave is the Scholte wave that propagates slower than all body waves. By comparing Figure 2a–2c, it can be seen that the formation transmitted S-wave exists and remains strong in the wireline and LWD models and the Scholte wave becomes the Stoneley wave in a borehole. The presence of the LWD tool has a strong impact on the formation P-wave, but it does not affect the transmitted S-wave significantly.

Figure 3 shows the recorded waveforms (pressure) at the receivers for the wireline and LWD models and the corresponding semblance of slowness-time-coherence (STC). STC is a method used for identifying and measuring the slowness and time of arrival of coherent acoustic waves propagating across an array of receivers. The leaky P-wave appears as a long wave train in the wireline model, whereas it becomes a compact wave packet in the LWD model. The dashed red lines indicate the transmitted S-wave recorded in the borehole fluid. It arrives a little bit earlier than the Stoneley wave. The appearance of the slow formation transmitted S-wave in the borehole contradicts the traditional ray theory. However, this phenomenon can be explained by Huygens' principle, which states that every point of a wavefront may be considered the source of secondary wavelets that spread out in all directions with a speed equal to the speed of propagation of the waves. Thus, the transmitted S-wave recorded in the borehole is the fluid particle motion induced by the formation S-wave at the wellbore. Although the transmitted S-wave looks relatively faint in the waveform data, it becomes prominent in STC after stacking because the signal is coherent and nondispersive. The transmitted S-wave and the Stoneley wave can be easily recognized in the LWD STC, but the two modes are not separated very well in the wireline STC. At first glance, the bright region corresponding to the transmitted S-wave in the wireline STC seems to belong to the Stoneley mode. LWD differs from wireline in STC analysis because of the change in Stoneley dispersion caused by the drill collar. Figure 4 shows the dispersion relations of the borehole modes calculated from the dispersion equations of the models (Rao and Vandiver, 1999). It can be seen that the slowness of the transmitted S-wave (denoted as S) is equal to the formation shear slowness (272 μs/ft) in both models. The Stoneley dispersion curve for the wireline model bends downward toward the formation shear slowness at low frequencies, resulting in the interference of the Stoneley and transmitted S-waves at low frequencies. However, the Stoneley dispersion curve changes toward the opposite direction for the LWD model, as shown in Figure 4b, resulting in better temporal separation of the Stoneley and transmitted S-waves. Thus, the transmitted S-wave becomes easier to be distinguished in the LWD STC. In Figure 4b, the dispersive modes less than 139 μs/ft are the tool modes induced by the drill collar.

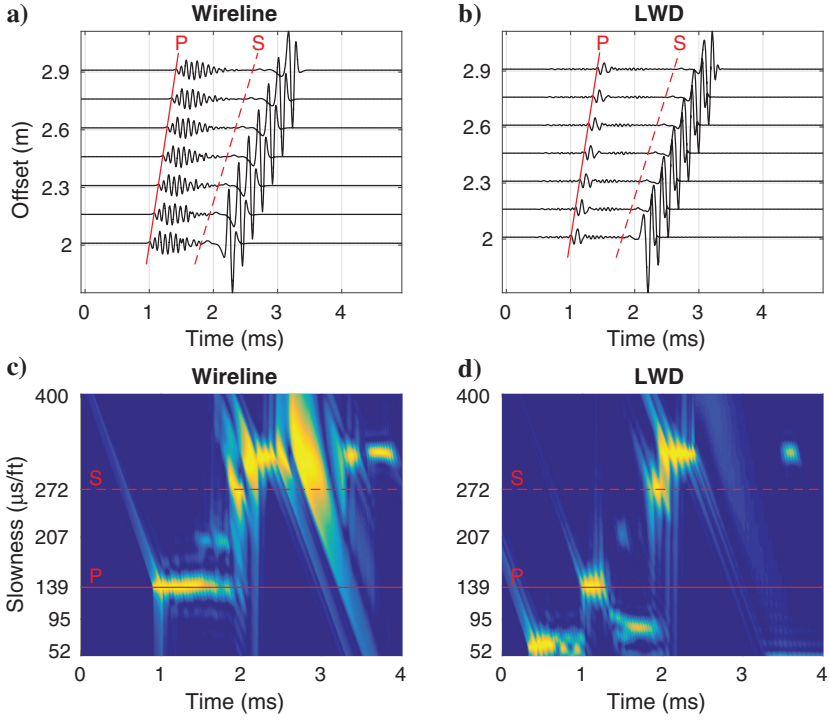

Figure 3. (a and b) Synthetic waveforms for the wireline and LWD models. The solid and dashed red lines mark the compressional and shear arrival times, respectively. The source center frequency is 8 kHz. (c and d) STC calculated from the waveforms.

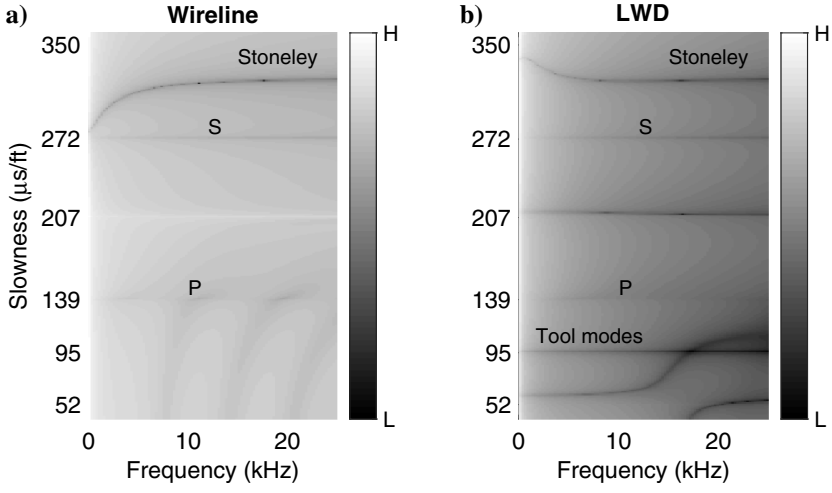

Figure 4. Dispersion relations calculated from the dispersion equation for the (a) wireline and (b) LWD models. The dark and light colors indicate low and high values, respectively. The lines/curves with low values (in black) indicate the modes excited in the borehole models. P and S indicate the P- and transmitted S-waves, respectively.

To use the transmitted S-wave to measure slow formation shear slowness, it needs to be separated from other waves in STC so that its slowness can be easily extracted. The dispersion analysis shown in Figure 4 indicates that Stoneley is the most important mode affecting the transmitted S-wave. The amount of separation between the Stoneley and transmitted S-waves in slowness determines how well the transmitted S-wave separates from the Stoneley in STC. This can be studied by analyzing the Stoneley slowness in the low- and high-frequency limits.

The low-frequency Stoneley wave is also called the tube wave, whose slowness in the limit of zero frequency is given as (Norris, 1990)

$$S_{\text{tube}} = S_f \cdot \sqrt{1 + a_F \frac{\rho_f S_f^{-2}}{\rho S_s^{-2}} + a_T \frac{\rho_f S_f^{-2}}{\rho_T S_T^{-2}}} \tag{1}$$

with

$$a_F = \frac{1}{1-f}, \tag{2}$$

$$a_T = \frac{f}{1-f} \cdot \frac{f_T + (1-\upsilon_T)/(1+\upsilon_T)}{1-f_T}, \tag{3}$$

$$f = \left(\frac{r_o}{R}\right)^2, \tag{4}$$

$$f_T = \left(\frac{r_i}{r_o}\right)^2, \tag{5}$$

where ρ, ρ_f, and ρ_T are the density of formation, borehole fluid, and drill collar, respectively; S_f is the fluid compressional slowness; S_S and S_T are the formation and the tool shear slownesses, respectively; ν_T is the tool's Poisson's ratio; f is the volume fraction of the tool in the borehole; f_T is the volume fraction of the inner part of the tool; and a_F and a_T are the factors controlling the influence of the formation and the tool on the tube wave slowness, respectively.

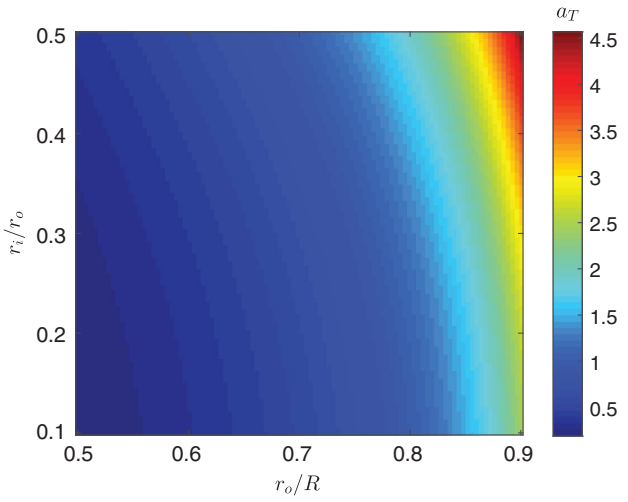

Figure 5. Variation of the value of a_T (equation 3) for different r_o/R and r_i/r_o ratios.

According to equation 1, the tube wave slowness is always larger than the borehole fluid slowness, but its relationship with the formation shear slowness depends on the formation properties and tool configuration. The drill collar thickness increases with increasing tool external radius r_o when the tool inner radius r_i is unchanged, or it would decrease with increasing r_i when r_o is fixed. In Figure 5, the variation of the tool factor a_T indicates that the value of a_T is strongly influenced by r_o, whereas it is less sensitive to r_i. A larger value of a_T means there is a greater tool effect. Thus, the ratio of

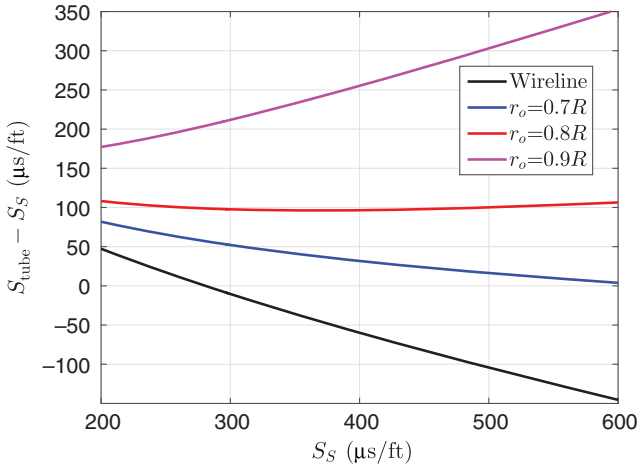

Figure 6. Difference between the tube wave slowness S_{tube} and the formation shear slowness S_S for different tool sizes when S_S varies from 200 to 600 μs/ft. The value of the tool inner radius is fixed in the calculation. The blue, red, and magenta curves show the slowness difference for tools of different outer radii, respectively. The black curve shows the slowness difference for the wireline case.

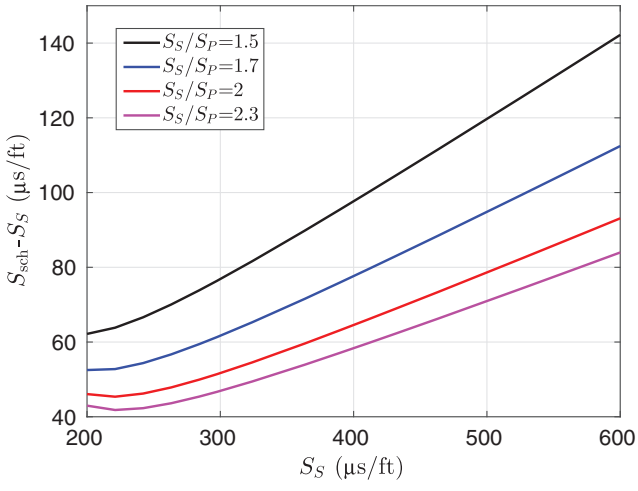

Figure 7. Difference between the Scholte wave slowness S_{sch} and the formation shear slowness S_S for different formation S_S/S_P ratios when S_S varies from 200 to 600 μs/ft. The other parameters in equation 6 are fixed in the calculation of S_{sch}.

tool size and hole size is an important factor affecting the tube wave slowness. Figure 6 shows the slowness separation between the tube wave and formation S-wave for tools of different size when the formation shear slowness varies from 200 to 600 μs/ft. The slowness difference S_{tube}-S_S increases with the tool size. For slow formations with $S_S < 300$ μs/ft, the slowness separation is 50–80 μs/ft with a slim tool ($r_o = 0.7R$) and it can go beyond 150 μs/ft with a large tool ($r_o = 0.9R$). For very slow formations ($S_S \sim 600$ μs/ft), a moderate-size tool ($r_o = 0.8R$) can make the tube wave slowness separate from the formation shear slowness by approximately 100 μs/ft. For the case of wireline (black curve), the slowness of the tube wave is very close to the formation shear slowness for small values of S_S. When $S_S > 280$ μs/ft, the tube wave slowness is below the formation shear slowness, resulting in the intersection between the dispersion curves of the Stoneley and transmitted S-waves. Therefore, it is difficult to distinguish the transmitted S-wave at low frequencies in wireline data due to the Stoneley interference. However, it is possible to detect the transmitted S-wave in LWD data because the presence of the drill collar can make the transmitted S-wave decouple from the Stoneley wave.

At high frequencies, the Stoneley dispersion curve asymptotically approaches the Scholte wave slowness, which satisfies the following equation (Zheng et al., 2013):

$$\frac{\rho_f}{4\rho} S_S^4 \sqrt{\frac{S_P^2 - S_{\text{sch}}^2}{S_f^2 - S_{\text{sch}}^2}} + \left(S_{\text{sch}}^2 - \frac{S_S^2}{2}\right)^2 + S_{\text{sch}}^2 \sqrt{(S_P^2 - S_{\text{sch}}^2)(S_S^2 - S_{\text{sch}}^2)} = 0, \quad (6)$$

where S_{sch} is the Scholte wave slowness; S_P and S_S are the formation compressional and shear slownesses, respectively; and S_f is the fluid slowness.

The Scholte wave slowness is obtained by numerically solving equation 6. The Scholte wave always exists for a fluid-solid interface, and its slowness is larger than all body wave slownesses (Zheng et al., 2013). Thus, the Stoneley wave slowness is always larger than the formation shear slowness at high frequencies. Figure 7 shows the slowness difference between the Scholte wave and the formation S-wave for formations with different S_S/S_P ratios when S_S varies from 200 to 600 μs/ft. For a wide range of S_S and S_P values, the separation of the Scholte wave and formation S-wave in slowness is considerably large (>40 μs/ft).

Based on the tube wave and Scholte wave analysis, we know that the transmitted S-wave can be decoupled from the LWD Stoneley wave and the amount of their separation in slowness

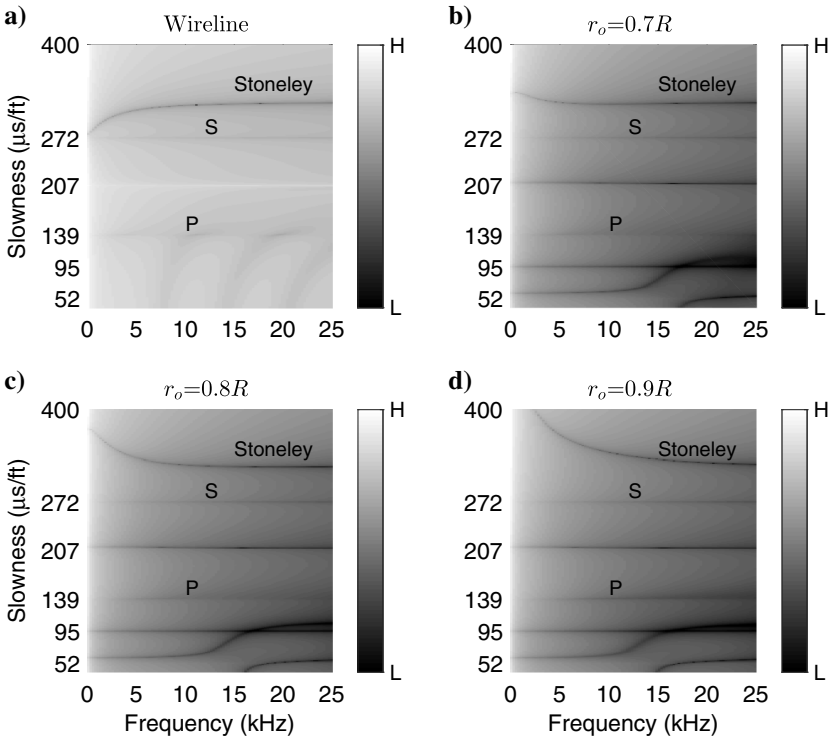

Figure 8. Dispersion relations for the (a) wireline model and (b-d) three LWD models of different tool outer radii. The R is the borehole radius.

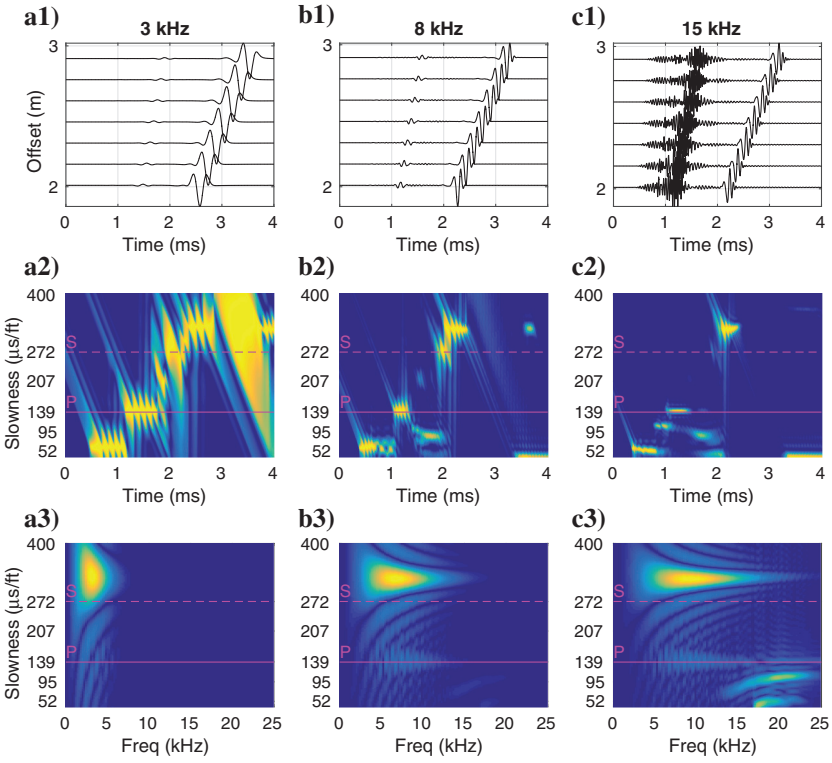

Figure 9. The LWD modeling results for sources of three different frequencies. The first row shows the waveforms. The second and third rows are the corresponding STC and SFC plots. The solid and dashed magenta lines indicate the formation compressional and shear slownesses, respectively. Normalization at each scanning time window is applied to the STC calculation, whereas there is no normalization in the SFC calculation.

mainly depends on the tool size and frequency. Figure 8 shows the dispersion relations for the wireline model (Figure 8a) and three LWD models (Figure 8b–8d) with different tool outer radii. All parameters for the LWD models are the same as those listed in Table 1 except for the tool outer radius. The behavior of the Stoneley dispersion for these four models is consistent with the previous theoretical analysis. The amount of separation between the Stoneley and transmitted S-waves increases with the tool size at low frequencies, whereas it remains unchanged at high frequencies.

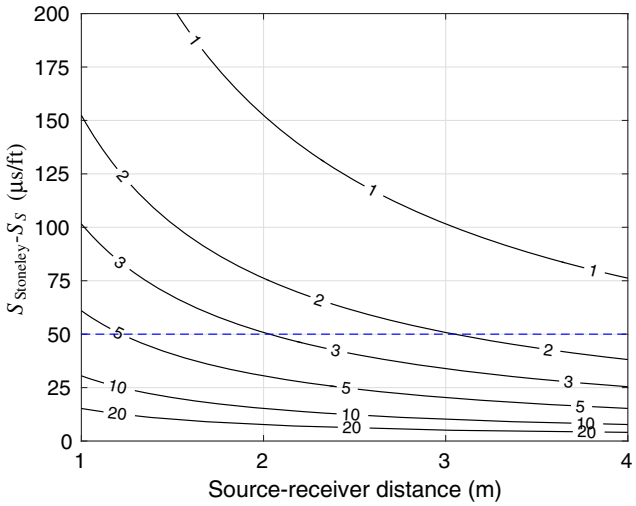

Figure 10. The allowed minimum data frequency (in kHz) to separate the Stoneley wave and transmitted S-wave in time.

Figure 9 shows the LWD modeling results for sources of different frequencies. Model parameters are given in Table 1. The first row shows the waveforms. The second and the third rows are the STC and the semblance of slowness-frequency-coherence (SFC), respectively (Nolte et al., 1997). SFC analysis is similar to STC analysis except that it is performed in the frequency domain. STC is normalized at each scanning time window, whereas there is no normalization applied to SFC. The amplitude of SFC represents the relative strength of different modes in the data. The Stoneley wave is always the dominant signal regardless of the source frequency. The tool modes are weak when the source frequencies are 3 and 8 kHz, but they become prominent when the source frequency increases to 15 kHz. The bright spot corresponding to the transmitted S-wave is well-separated from the Stoneley in the STC for the 8 kHz source. For the case of the 3 kHz source, there is some interference between the transmitted S-wave and the Stoneley wave. This is caused by the increase of signal's period with a lower source frequency. If we assume that the traveltime difference between the Stoneley and transmitted S-waves needs to be at least one period to separate them in STC analysis, then the minimum frequency of the signals needs to satisfy

$$f_{\min} = \frac{1}{x \cdot (S_{\text{Stoneley}} - S_S)}, \tag{7}$$

where x is the source-receiver distance.

Figure 10 shows the relationship among $f_{\min}$, source-receiver distance, and the slowness difference, S_{Stoneley}-S_S. In our models, the source-receiver distance is 2–3 m and the slowness difference S_{Stoneley}-S_S is approximately 50 μs/ft, so the allowed minimum frequency of the data is approximately 3 kHz. Because the slowness difference is generally larger than 40 μs/ft, as shown in Figures 6 and 7, the transmitted S-wave should be able to be decoupled from the Stoneley wave in STC analysis in most cases if the minimum frequency of the data is higher than approximately 5 kHz. In Figure 9a2, the interference between the Stoneley and transmitted S-waves is caused by the waves at a frequency smaller than 3 kHz. For the simulation of a 15 kHz source, the transmitted S-wave is hard to recognize in STC, as shown in Figure 9c2, because it is overwhelmed by the tool modes that become strong above 15 kHz, as shown in the SFC of Figure 9c3.

The dispersion relations shown in Figure 8 suggest that there is a mode at fluid slowness (207 μs/ft). In Figure 9a2 and 9b2, we can see that there are small bright spots at 207 μs/ft, which correspond to the fluid mode. To investigate whether the fluid mode would affect the transmitted S-wave when their slownesses are close to each other, we build another model with $S_P = 112$ μs/ft and $S_S = 220$ μs/ft while keeping the other model parameters the same as the

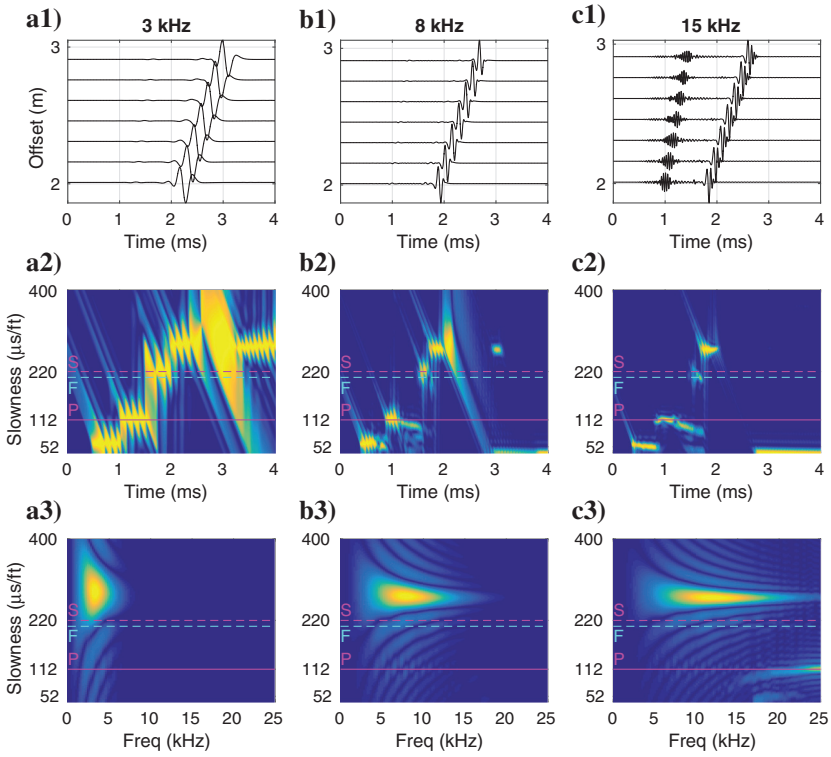

Figure 11. The same as Figure 9 except that the formation compressional and shear slownesses are changed to 112 and 220 μs/ft, respectively. The cyan dashed line (F) indicates the borehole fluid slowness (207 μs/ft).

previous model. The modeling results for sources of 3, 8, and 15 kHz center frequencies are shown in Figure 11. For the cases of 3 and 8 kHz sources, the fluid mode has little effect on the transmitted S-wave in STC analysis because it is very weak. When the source frequency increases to 15 kHz, the fluid mode becomes as strong as the transmitted S-wave, so it can affect the transmitted S-wave in STC analysis at high frequencies.

FIELD EXAMPLES

Zemanek et al. (1984) conduct a comparison of data measured by a long spaced monopole logging tool and their in-house-designed dipole tool in a slow formation. The frequency of the source is approximately 1 kHz. Figure 12 shows a comparison of a data set measured at the far receiver 15 ft away from the transmitter. Their core data indicate that the rock in the section between 4900 and 5100 ft is either very poorly consolidated or completely unconsolidated. There is no clear evidence of S-wave arrival on the monopole variable density logs (VDLs). Thus, this section is interpreted as a slow formation. We obtain the S-wave arrival time from the dipole VDL (right figure) that shows distinct flexural wave signals. The dashed red curve on the dipole VDL delineates the estimated arrival time of the flexural wave. On the monopole VDL, besides the P-wave (P) and the Stoneley wave (T), there is another wave arriving in between at approximately 3.5 ms. Because this wave is relatively weaker than other waves and this section of the formation is a slow formation, it is not considered as a formation wave by Zemanek et al. (1984). The overlay of the flexural wave arrival time on the monopole VDL (dashed red curve in Figure 12) indicates that the arrival time of the wave at approximately 3.5 ms is consistent with that of the dipole flexural wave. The arrival time of this wave varies with depth, and it is slower than the fluid signals that are highlighted by the circle, so it is not associated with the fluid waves whose arrival time should be invariant for constant transmitter-to-receiver distance. Therefore, we interpret this wave as the formation transmitter S-wave. Because the transmitter-to-receiver distance is pretty large (15 ft), the Stoneley wave and the transmitted S-wave have very good temporal separation (approximately 0.5 ms).

Figure 13 shows the data acquired at depths below the section of Figure 12. Again, the formation transmitted S-wave can be seen on the monopole VDL, and its arrival time is consistent with that of the dipole flexural wave at greater than 5200 ft. However, the flexural wave lags behind the transmitted S-wave by about a quarter millisecond between 5220 and 5300 ft. In this section, the dipole VDL shows strong high-frequency fluid signals that arrive ahead of the flexural wave, and the monopole and dipole data have very poor quality above and below this section. This indicates that the borehole conditions are complicated in this section. Thus, the data recorded at these depths may not be reliable. Without the original sonic waveforms and additional information about the borehole conditions, it is hard to find out the cause of the difference in the monopole and dipole S-wave arrival time based on the VDL results.

Despite the uncertain section in Figure 13, the results shown in Figures 12 and 13 are promising. These field examples demonstrate that the slow formation transmitted S-wave can be detected by a

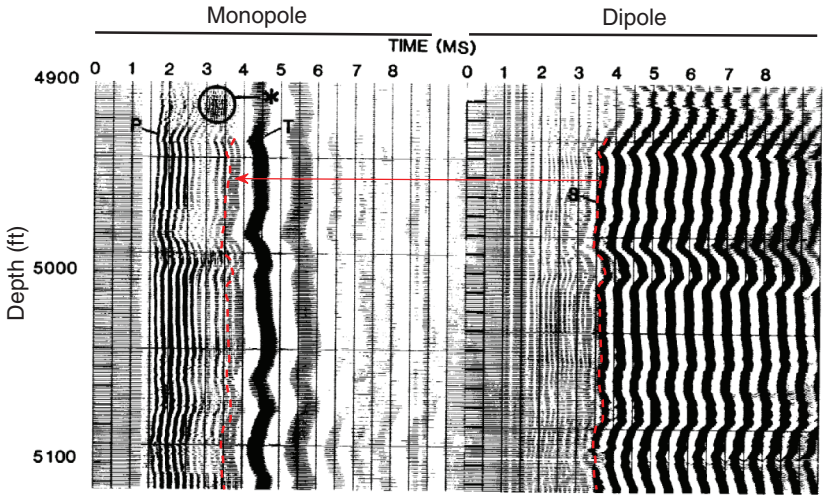

Figure 12. An example of monopole (left) and dipole (right) VDL acquired in a slow formation (modified from Zemanek et al., 1984). The distance between the transmitter and receiver is 15 ft for both tools. The P, S, and T indicate the P-wave, dipole flexural wave, and Stoneley wave, respectively. The signals highlighted by the circle are the high-frequency fluid-borne energy. The dashed red curve on the dipole VDL delineates the flexural wave arrival time, which is overlaid on the monopole VDL for comparison.

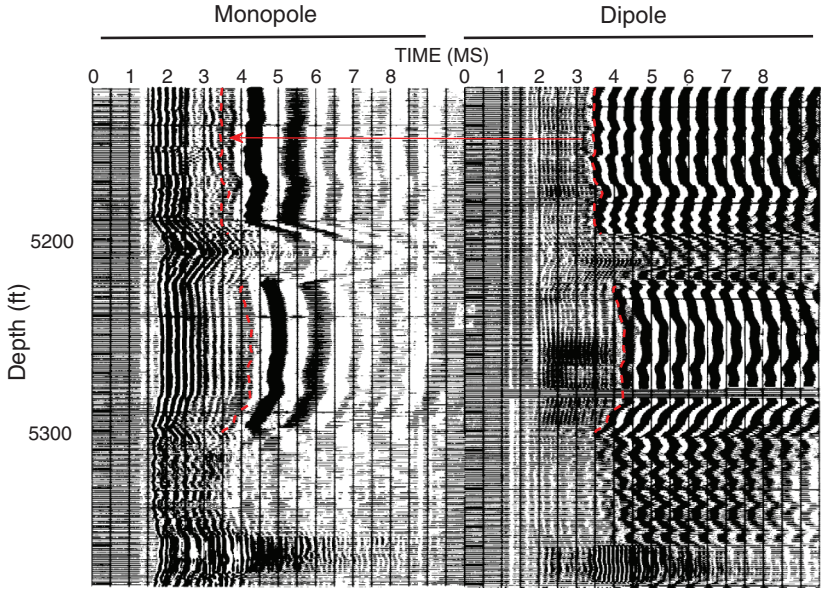

Figure 13. The same as Figure 12 except for a section below that of Figure 12 (modified from Zemanek et al., 1984). Note that the errors in the tick labels of the time axis in the original figure of Zemanek et al. (1984) have been corrected.

monopole acoustic tool and this wave can provide information about formation shear slowness.

CONCLUSION

Through numerical and theoretical analyses, we have shown that the transmitted S-wave generated by a monopole LWD tool can be detected in sonic data because the transmitted S-wave can be decoupled from the Stoneley wave in the LWD environment. However, the transmitted S-wave is hard to detect in wireline logging due to the Stoneley interference. Although the transmitted S-wave is weak, its nondispersive nature makes it suitable for shear slowness measurements. This may provide a data-based approach to determine the slow formation shear slowness using monopole LWD, which complements the quadrupole method in LWD analysis. Moreover, this study brings new insight into the characteristic of borehole S-wave propagation under LWD conditions. We found that the optimal source frequency range to have the transmitted S-wave separated from other waves in STC analysis is approximately 5–10 kHz. Below this frequency range, the transmitted S-wave could interfere with the Stoneley wave at near offsets, making it difficult to separate them in STC analysis. At high frequencies (>10 kHz), the transmitted S-wave can be overwhelmed by the tool modes. We also analyzed two field examples that demonstrate the existence of slow formation transmitted S-wave in monopole data.

ACKNOWLEDGMENTS

We thank Y. Zheng for the enlightening discussion about Scholte wave propagation. A. Cheng is supported by funding from the EDB Petroleum Engineering Professorship program at National University of Singapore. This work is supported by the National Natural Science Foundation of China (grant no. 41704112).

REFERENCES

Chen, S., 1989, Shear-wave logging with quadrupole sources: Geophysics, **54**, 590–597, doi: 10.1190/1.1442686.

Fang, X., M. C. Fehler, and A. Cheng, 2014, Simulation of the effect of stress-induced anisotropy on borehole compressional wave propagation: Geophysics, **79**, no. 4, D205–D216, doi: 10.1190/geo2013-0186.1.

Jørgensen, O., and D. Burns, 2013, Novel finite-element approach applied to borehole quadrupole dispersion analysis in stress-sensitive formations: Geophysics, **78**, no. 6, D499–D509, doi: 10.1190/geo2012-0487.1.

Nolte, B., R. Rao, and X. Huang, 1997, Dispersion analysis of split flexural waves: Massachusetts Institute of Technology, Earth Resources Laboratory Annual Consortium Meeting.

Norris, A. N., 1990, The speed of a tube wave: The Journal of the Acoustical Society of America, **87**, 414–417, doi: 10.1121/1.399262.

Rao, R. V. N., and J. K. Vandiver, 1999, Acoustics of fluid-filled boreholes with pipe: guided propagation and radiation: Journal of the Acoustical Society of America, **105**, 3057–3066, doi: 10.1121/1.424635.

Su, Y. D., X. M. Tang, C. X. Zhuang, S. Xu, and L. Zhao, 2013, Mapping formation shear-velocity variation by inverting logging-while-drilling quadrupole wave dispersion data: Geophysics, **78**, no. 6, D491–D498, doi: 10.1190/geo2013-0136.1.

Syresin, D., N. Sakiyama, H. Yamamoto, R. Iritani, and H. Nakajima, 2016, Characterization of azimuthal slowness sensitivity for LWD unipole tools: Presented at the SPWLA 57th Annual Logging Symposium.

Tang, X. M., and C. Cheng, 2004, Quantitative borehole acoustic methods: Elsevier.

Tang, X. M., V. Dubinsky, T. Wang, A. Bolshakov, and D. Patterson, 2002, Shear velocity measurement in the logging-while-drilling environment: Modeling and field evaluations: Presented at the SPWLA 43rd Annual Logging Symposium.

Tang, X. M., Y. Zheng, and V. Dubinsky, 2004, Logging while drilling acoustic measurement in unconslidated slow formations: Presented at the SPWLA 46th Annual Logging Symposium.

Varsamis, G. L., L.T. Wisniewski, A. Arain, and G. Althoff, 1999, A new MWD full wave dual mode sonic tool design and case histories: Presented at the SPWLA 40th Annual Logging Symposium.

Wang, H., G. Tao, and M. Fehler, 2015, Investigation of the high-frequency wavefield of an off-center monopole acoustic logging-while-drilling tool: Geophysics, **80**, no. 4, D329–D341, doi: 10.1190/geo2014-0426.1.

Wang, T., M. Dawber, and P. Boonen, 2011. Theory of unipole acoustic logging tools and their relevance to dipole and quadrupole tools for slow formations: Presented at the SPE Annual Technical Conference and Exhibition.

Wang, T., and X. Tang, 2003a, Finite-difference modeling of elastic wave propagation: A nonsplitting perfectly matched layer approach: Geophysics, **68**, 1749–1755, doi: 10.1190/1.1620648.

Wang, T., and X. Tang, 2003b, Investigation of LWD quadrupole shear measurement in real environments: Presented at the SPWLA 44th Annual Logging Symposium.

Zemanek, J., F. A. Angona, D. M. Williams, and R. L. Caldwell, 1984, Continuous acoustic shear wave logging: Presented at the SPWLA 25th Annual Logging Symposium.

Zhang, Z., M. Mochida, M. Kubota, H. Yamamoto, and T. Endo, 2010, Shear slowness estimation by inversion of LWD borehole quadrupole mode: 80th Annual International Meeting, SEG, Expanded Abstracts, 528–532.

Zheng, Y., X. Fang, J. Liu, and M. C. Fehler, 2013, Scholte wave generated by seafloor topography: Massachusetts Institute of Technology, Earth Resources Laboratory Annual Consortium Meeting.

Zhu, Z., M. N. Toksöz, R. Rao, and D. R. Burns, 2008, Experimental studies of monopole, dipole and quadrupole acoustic logging while drilling (LWD) with scaled borehole models: Geophysics, **73**, no. 4, E133–E143, doi: 10.1190/1.2919827.